

Journal of Biomedical Optics

SPIDigitalLibrary.org/jbo

Evaluation of the role of CD207 on Langerhans cells in a murine model of atopic dermatitis by *in situ* imaging using Cr:forsterite laser-based multimodality nonlinear microscopy

Jyh-Hong Lee
Ming-Rung Tsai
Chi-Kuang Sun
Bor-Luen Chiang

Evaluation of the role of CD207 on Langerhans cells in a murine model of atopic dermatitis by *in situ* imaging using Cr:forsterite laser-based multimodality nonlinear microscopy

Jyh-Hong Lee,^a Ming-Rung Tsai,^b Chi-Kuang Sun,^{b,c} and Bor-Luen Chiang^{a,d}

^aNational Taiwan University Hospital and National Taiwan University College of Medicine, Department of Pediatrics, Taipei, 10002, Taiwan

^bNational Taiwan University, Graduate Institute of Photonics and Optoelectronics and Department of Electrical Engineering, Taipei, 10617, Taiwan

^cResearch Center for Applied Sciences, Academia Sinica, Taipei, 11529, Taiwan

^dNational Taiwan University College of Medicine, Graduate Institute of Clinical Medicine, Taipei, 10002, Taiwan

Abstract. Atopic dermatitis (AD) is an allergic inflammatory disease of skin. It remains unclear that CD207 of Langerhans cells (LCs) plays a central role in the development of allergic sensitization. There is little data on LCs within the microenvironment *in vivo*. We used a murine model of epicutaneous (EC) ovalbumin (OVA) sensitization inducing an inflammatory skin resembling AD to explore the role of CD207 in the pathogenesis of AD. Cr:forsterite laser-based multimodality nonlinear microscopy was applied for *in situ* imaging. Peritoneal injections of Alexa Fluor 647-rat anti-mouse CD207 into mice were performed to specifically trace the LCs. Peritoneal injections of OVA-Alexa Fluor 647 conjugate into mice were performed to specifically trace the OVA. We found that combining Alexa Fluor fluorescent probes with multimodality nonlinear microscopy permitted the unequivocal *in situ* imaging of CD207-expressing LCs. The relevant time-course, expressional, and functional studies reveal that CD207 of LCs plays an essential role during the induction of EC sensitization. We establish and validate that Cr:forsterite laser-based multimodality nonlinear microscopy is applicable for the specific detection of labeled mAb-bound LCs and labeled antigen. We suggest that CD207-expressing LCs initiate the allergic response through the CD207 mediated epicutaneous sensitization associated with the development of AD. © 2012 Society of Photo-Optical Instrumentation Engineers (SPIE). [DOI: 10.1117/1.JBO.17.11.116007]

Keywords: atopic dermatitis; CD207; epicutaneous sensitization; *in vivo* imaging; langerin; Langerhans cell; murine model; ovalbumin; two-photon fluorescence.

Paper 12439 received Jul. 11, 2012; revised manuscript received Sep. 27, 2012; accepted for publication Oct. 1, 2012; published online Nov. 1, 2012.

1 Introduction

Atopic dermatitis (AD) is a chronic inflammatory disease associated with cutaneous hyperreactivity to environmental triggers.¹ AD is characterized by eczematous lesions and in some cases are associated with elevated serum IgE levels. Various studies have indicated that AD has a complex etiology, with activation of multiple immunologic and inflammatory pathways.^{2,3} Langerhans cells (LCs) are the predominant dendritic cell (DC) population in the epidermis and are thus the first line of defense against antigens that penetrate the skin.⁴ In AD skin lesions, the majority of LCs exhibit surface-bound IgE, with FcεRI being the critical IgE-binding receptor enabling it to capture allergens penetrating into the skin. LCs up-regulate their display of FcεRI in atopy patch tests.⁵ In AD, FcεRI⁺ LCs bearing the antigen migrate from the skin to the draining lymph nodes (DLNs) where they activate FcεRI-mediated Th2 immune responses. It is possible that other undefined receptor-mediated antigen sensitization pathways might thus be responsible for allergen uptake and allergic response relevant to the pathophysiology of AD.

CD207 (langerin) is a type II C-type lectin receptor (CLR) that binds mannose and related sugars in a calcium-dependent manner through its carbohydrate-recognition domain (CRD).⁶ Its expression is demonstrated at the surface membrane as well as in Birbeck granules, those organelles specific for LCs. Several lines of evidence have indicated that CD207 is a specific marker for the acquisition of the LC phenotype.^{7,8} A mouse homologue of human CD207 has also been identified.^{9,10} The predicted mouse CD207 displays an overall 66% sequence identity with the human CD207.⁹ It has been suggested that the process of antigen capture, internalization (endocytosis), the formation of Birbeck granules, processing, migration to lymphoid tissue, and maturation of LCs is a consequence of CD207 function.¹¹

The precise role of LCs in allergic diseases is still under debate. A concordant increase in LC proliferation in patients with human AD and in a mouse AD model suggests a potential relevance of LCs in the pathophysiology of AD.^{12,13} LCs are in the foreground in the initial sensitization phase of AD.^{14,15} CD207 expression was essential for promotion of the skin allergic responses.¹⁶ However, LCs contribute to Th2 polarization by an unknown mechanism after allergen capture.¹⁷ It is not clear

Address all correspondence to: Bor-Luen Chiang, National Taiwan University Hospital, Department of Pediatrics, 7 Chung-Shan South Road, Taipei 10002, Taiwan. Tel: 886-2-23123456 ext. 67302; Fax: 886-2-23972031; E-mail: gicmbor@ntu.edu.tw

that whether allergen uptake by CD207 plays any role in the development of allergic sensitization in human beings.¹⁸

We set up a technique combining Alexa Fluor conjugates with Cr:forsterite laser-based multimodality nonlinear microscopy to allow for the unequivocal imaging of LCs and ovalbumin (OVA) in the skin and in the DLNs.

2 Materials and Methods

2.1 Mice, Allergens, and Epicutaneous Sensitization

For the animal model of epicutaneous (EC) OVA sensitization, six- to eight-week-old female BALB/c mice were obtained from the Animal Center of the College of Medicine, National Taiwan University. All procedures performed on the mice were approved by The Animal Care and Use Committee of National Taiwan University Hospital. EC sensitization of the mice was performed as previously described.¹⁹ The protein antigens used in this study were OVA (100 mg/ml) (Sigma Chemical Co., St. Louis, MO, USA). The antigen was prepared in distilled water. In brief, 20 μ l of OVA solution was first added to the paper disc insert of a Finn Chamber (Epitest Co., Tuusula, Finland), which was then applied to a 1-cm² patch of sterile gauze. The disc was then applied to the skin on the lateral side of the abdomen and fixed and secured with an elastic bandage to ensure skin contact and to prevent oral ingestion. The OVA patches were kept there for 24 h and freshly prepared patches were reapplied to the same skin site everyday. The course of immunization was totally for five days.

2.2 Monoclonal Antibodies

Alexa Fluor 647-rat anti-mouse CD207, and Alexa Fluor 647-rat IgG2a isotype control were purchased from eBioscience, Inc. (San Diego, CA). OVA-Alexa Fluor 647 conjugate was purchased from Invitrogen (Carlsbad, CA). Alexa Fluor 700-rat anti-mouse CD205 was obtained from AbD Serotec (Oxford, UK).

2.3 Cr:forsterite Laser-Based Multimodality Nonlinear Microscopy System

The imaging system used for our experiments has been described previously.¹⁹ The Cr:forsterite laser-based multimodality nonlinear microscopy system was adapted from a FluoView 300 (FV300) scanning unit (Olympus, Tokyo, Japan) combined with a BX51 microscope (Olympus, Tokyo, Japan). The light source was a home-built Cr:forsterite fs laser centered at 1230 nm with a 130 fs pulse width and a 110-MHz repetition rate. The infrared (IR) beam exiting the laser was first shaped by a telescope and then directed into the Olympus FV300 scanning unit and the Olympus BX51 microscope. Real-time *x-y* scanning was accomplished with a pair of galvanometer mirrors inside the scanning unit. An IR water-immersion objective of working distance 2 mm (LUMplanFL/IR 60 \times /N.A. 0.9, Olympus, Tokyo, Japan) was used to focus the laser beam into the observed skin specimen. The average illumination power applied onto the surface of the specimen was 100 mW. A mean power of 100 mW with a 110-MHz repetition rate was chosen (pulse energy of \approx 0.91 nJ). Different optical harmonic signals were separated with another beam-splitter (BS 1, 490DRXR, Chroma technology, Rockingham, VT). The backward-propagating harmonic signals were detected by different photomultiplier tubes (PMT) (Harmamatsu R4220P for third harmonic generation (THG); and Harmamatsu R943-02 for second harmonic generation (SHG), Bridgewater, Westport, CT, USA) with 410- and 615-nm narrowband interference filters (D410/30X and D615/10X, respectively, Chroma technology) in front, which were synchronized with the galvanometer mirrors. For *in vivo* observation, the laser beam exiting the objective was scanned across the specimen and the backward-propagating multimodal nonlinear signals from the specimen were collected with the same water-immersion objective. The microscope objective employed to focus the laser beam also acted as the collection lens to collect the backward propagation SHG, THG, and two-photon fluorescence (TPF).

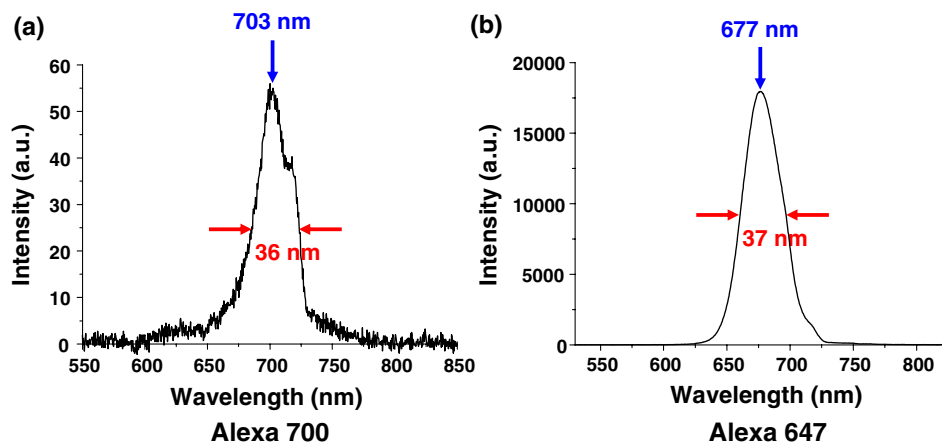


Fig. 1 Emission spectra obtained from the skin surface ($z = 0$) of mice under excitation wavelength 1230 nm of the Cr:forsterite fs laser. (a) emission spectrum of TPF acquired from Alexa Fluor 700-rat anti-mouse MHC Class II mAb with the peak emission wavelength at 703 nm; (b) emission spectrum of TPF acquired from Alexa Fluor 647-rat anti-mouse CD207 mAb with the peak emission wavelength at 677 nm. The Alexa Fluor 700-rat anti-mouse MHC Class II mAb and Alexa Fluor 647-rat anti-mouse CD207 mAb used for molecular labeling were injected 6 h before *in vivo* imaging in a concentration of 0.5 μ g/gm mice body weight. BALB/c mice were anesthetized and the hairs of their skin were removed. The objectives were in contact with the skin of the mice, and their interface was rinsed with distilled water. Optical sectioning of mice skin was carried out on the lateral side of the abdomen. Under the excitation wavelength 1230 nm of the Cr:forsterite fs laser, the backward propagation TPF was collected into a monochromator (SpectraPro-150, Roper Scientific) and recorded by a TE-cooled CCD detector (DV42-0E, Andor Technology). The monochromator is SpectraPro-150 spectrograph with a wavelength range of 0 to 1400 nm, yielding a resolution of 0.4 nm or better. $z =$ depths in μ m measured from the surface of capsule. The intensity counts are in arbitrary unit. TPF (two-photon fluorescence).

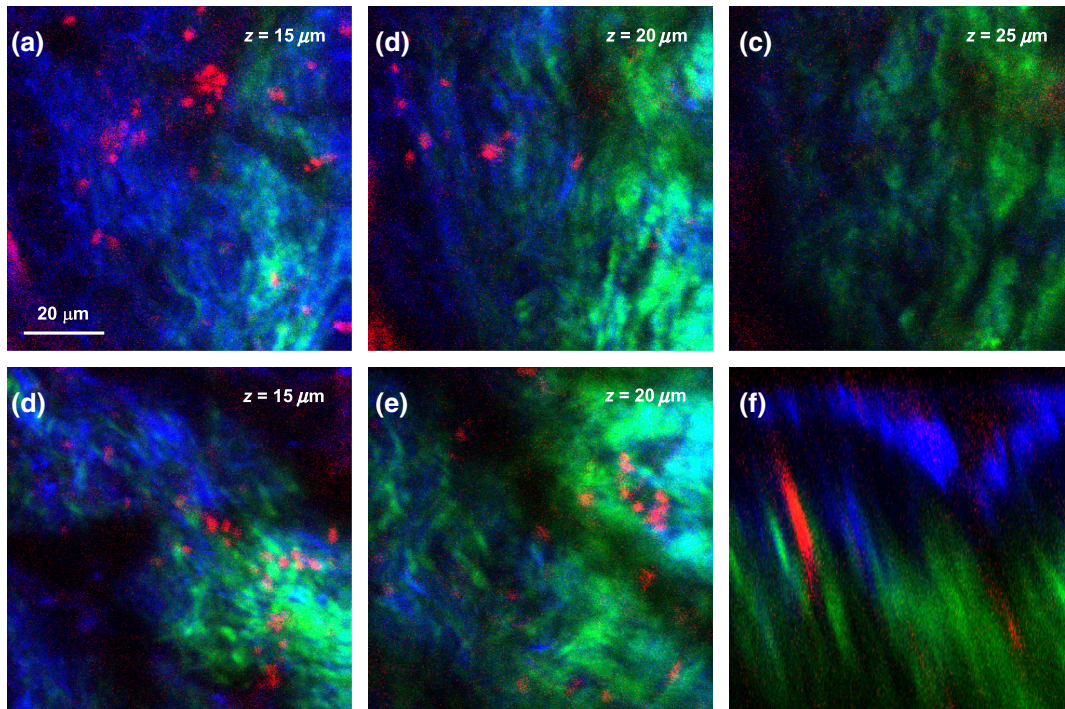


Fig. 2 Multimodal nonlinear images from skin of BALB/c mice received Alexa Fluor 700-rat anti-mouse MHC Class II mAb. (a) to (c) The x - y plane sectioning images from the basal epidermis (a); epidermo-dermal junction (b); and superficial dermis (c) of fixed skin, respectively. Some red spot mapped by TPF signals are noted within the epidermis mapped by THG signals (blue) and the upper dermis is mapped by SHG signals (green). (d) to (e) The x - y plane sectioning images from the epidermo-dermal junction of skin *in vivo*; (f) the x - z plane sectioning images from the whole layer of skin *in vivo*. The red spot signals located near the spinosum layer of epidermis is noted. z = depths in μm measured from skin surface. Scale bar: 20 μm . Data are representative images of three mice.

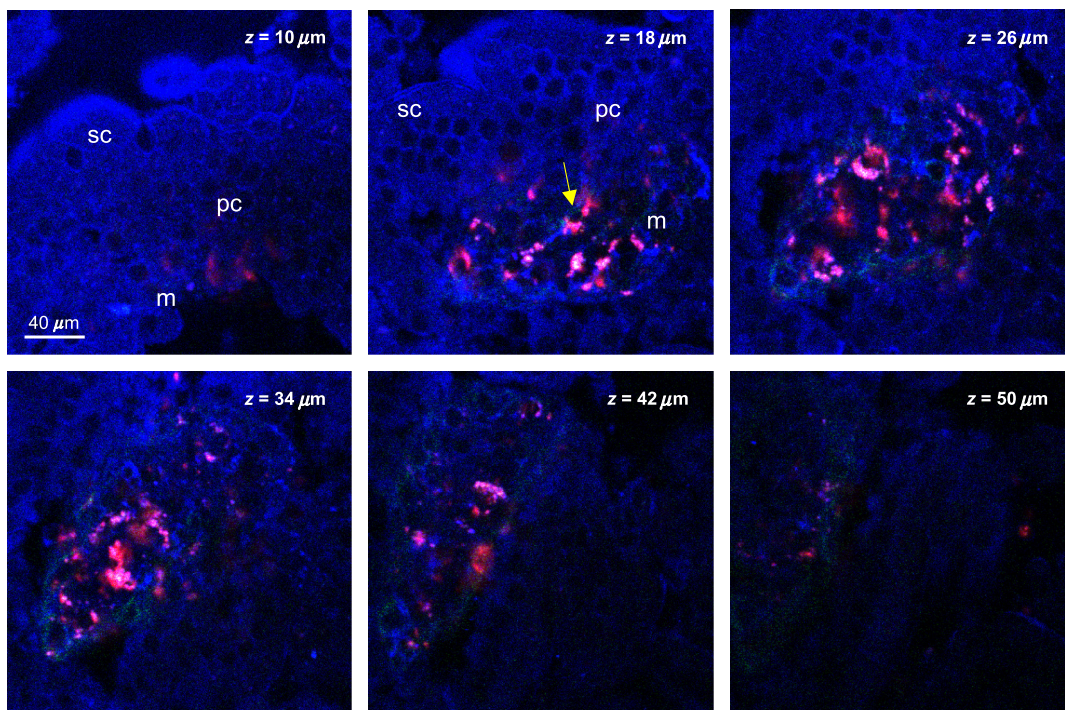


Fig. 3 Multimodal nonlinear images from skin-draining lymph node of BALB/c mice received Alexa Fluor 700-rat anti-mouse MHC Class II mAb. Representative x - y plane sectioning images of at various depths of fixed lymph node. The THG signals (blue) outlining the parenchyma of the lymph node are noted. The red TPF signals outlining the cellular morphology with some dendrites (yellow arrow) are clustered mainly within the inner paracortex area. z = depths in μm measured from skin surface. Scale bar: 40 μm . Data are representative image of three mice in each group. sc, superficial cortex; pc, paracortex; m, medullary sinus; THG, third harmonic generation.

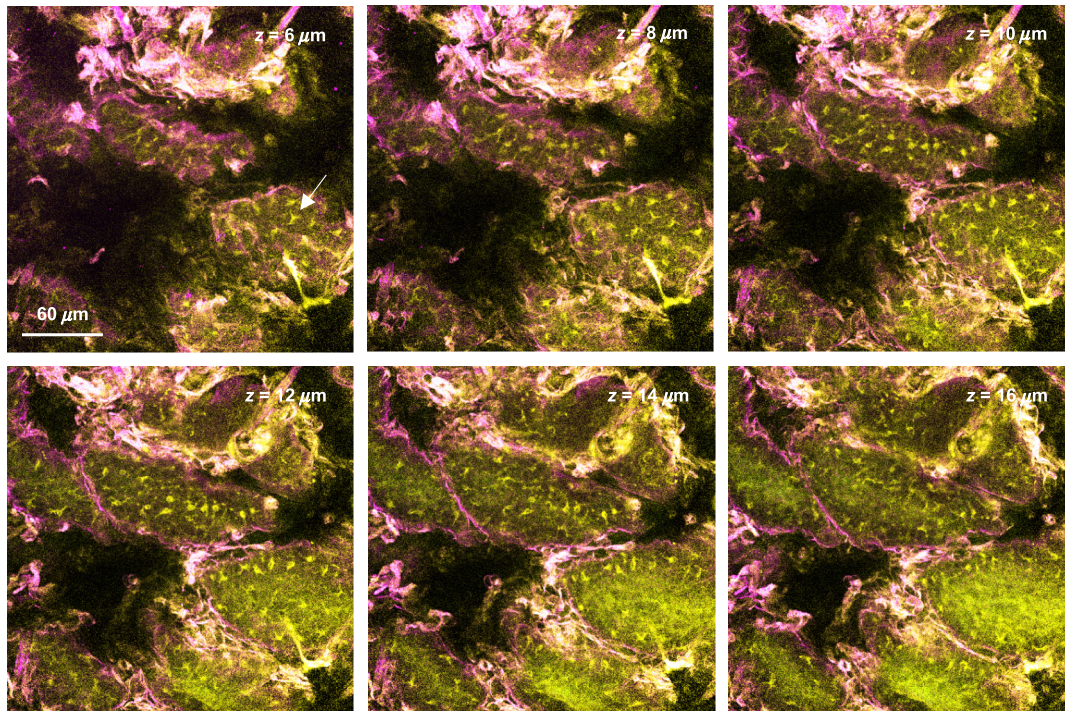
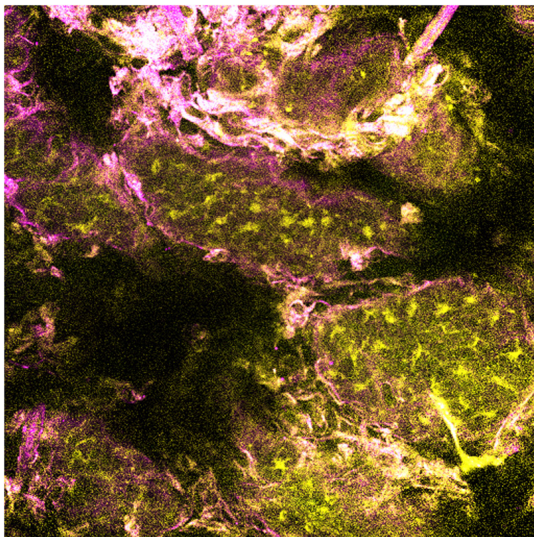


Fig. 4 Multimodal sequential sectioning images along the x - y plane from the surface of the fixed skin of BALB/c mice received Alexa Fluor 647-rat anti-mouse CD207 mAb. The morphology, approximated size and distribution of LCs are outlined by the TPF (light green) from the Alexa Fluor 647-rat anti-mouse CD207 mAb. The average size of the cell body of LCs were $13.4372 \pm 3.1458 \mu\text{m}$. LCs within the epidermis are distributed evenly at a density of around $1116.7336 \pm 127.8320 \text{ cells}/\text{mm}^2$. The autofluorescence (white) associated with the thickened stratum corneum of epidermis mapped by THG signals (purple) are observed.¹⁹ z = depths in μm measured from skin surface. Scale bar: $60 \mu\text{m}$. Data are representative image of three mice.



Video 1 *In vitro* movies of depth-resolved x - y plane sectioning images from the normal skin of BALB/c mice received Alexa Fluor 647-rat anti-mouse CD207 mAb. The epidermis is mapped by THG (purple) signals. The autofluorescence (white) associated with the thickened stratum corneum of epidermis are observed. The dermis is mapped by SHG (green) signals. The CD207-expressing LCs is mapped by TPF (yellow) signals. The CD207-expressing LCs observed in the epidermis are in groups and displayed the typical morphology of many extruding dendrites (MOV, 11.8 MB) [URL: <http://dx.doi.org/10.1117/1.JBO.17.11.116007.1>].

The backward-propagating TPF signals, which were not deflected with the dichroic mirror, were separated with another beam-splitter (BS 2, 865dcxru, Chroma technology) and detected by another PMT (Harmamatsu R928P). We employed long-pass emitter LF635/LP-A-000 (Semrock) and E700lp (Chroma technology) in front of the PMT for TPF to select wavelengths longer than 655 and 700 nm and block shorter wavelengths, respectively. We used short-pass emitter E700sp-2p (Chroma Technology), which transmits wavelengths shorter than 700 nm and blocks longer wavelengths. The scanning rate of the FV300 scanning unit was 1000 lines/s corresponding to two frames per second for a 512×512 pixel resolution. Spatial resolution was $\approx 500 \text{ nm}$ and $\approx 410 \text{ nm}$ for SHG and THG signals in the x - y plane, respectively. Resolution was on the order of $1 \mu\text{m}$ in the x - z plane. Specimens were mounted on a fixed stage within the microscope. Optical observations were made as follows:

- (1) *In vitro* imaging of fixed skin and lymph node specimens from normal and AD mice: The Alexa Fluor 700-rat anti-mouse major histocompatibility class (MHC) Class II, Alexa Fluor 647-rat anti-mouse CD207 (langerin), and Alexa Fluor 647-rat IgG2a isotype control (IC) mAb used for molecular labeling were injected 24 h before sacrifice in a concentration of $1 \mu\text{g}$ conjugated mAb/gm mice body weight. Paired measurements of both the OVA-treated and the untreated skin of the same mouse were performed. The skin DLNs were also obtained simultaneously. The skin and DLNs specimens used were fixed in

10% formaldehyde and were placed on the slide and then on the stage of the microscope.

- (2) *In vivo* imaging of skin and lymph node specimens from normal and AD mice: The Alexa Fluor 700-rat anti-mouse MHC Class II, Alexa Fluor 647-rat anti-mouse CD207 (langerin), and Alexa Fluor 647-rat IgG2a isotype control mAb used for molecular labeling were injected 6 h before *in vivo* imaging in a concentration of 0.5 ug/gm mice body weight. OVA-Alexa Fluor 647 conjugate was injected 6 h before *in vivo* imaging in a concentration of 10 ug/gm mice body weight. BALB/c mice were anesthetized with 150 μ l pentobarbital (10 mg/ml), and the hairs of their skin were removed with a hair remover. The objectives were in contact with

the skin of the mice and their interface was rinsed with distilled water. Optical sectioning of *in vivo* mice skin treated with OVA and that of control mice were carried out on the lateral side of the abdomen, which was placed on a special stage suitable for *in vivo* observation. The skin DLNs were obtained after the imaging of the skin was complete, and we observed the excised skin DLNs *ex vivo*.

2.4 Measurement of Cellular Numbers and CD207 Expression of Langerhans Cells Labeled with Alexa Fluor 647-Rat Anti-Mouse CD207

LCs are located at an average depth of $14.9 \pm 2.3 \mu\text{m}$.²⁰ We collected the acquired images from the skin at a depth of 15 μm and

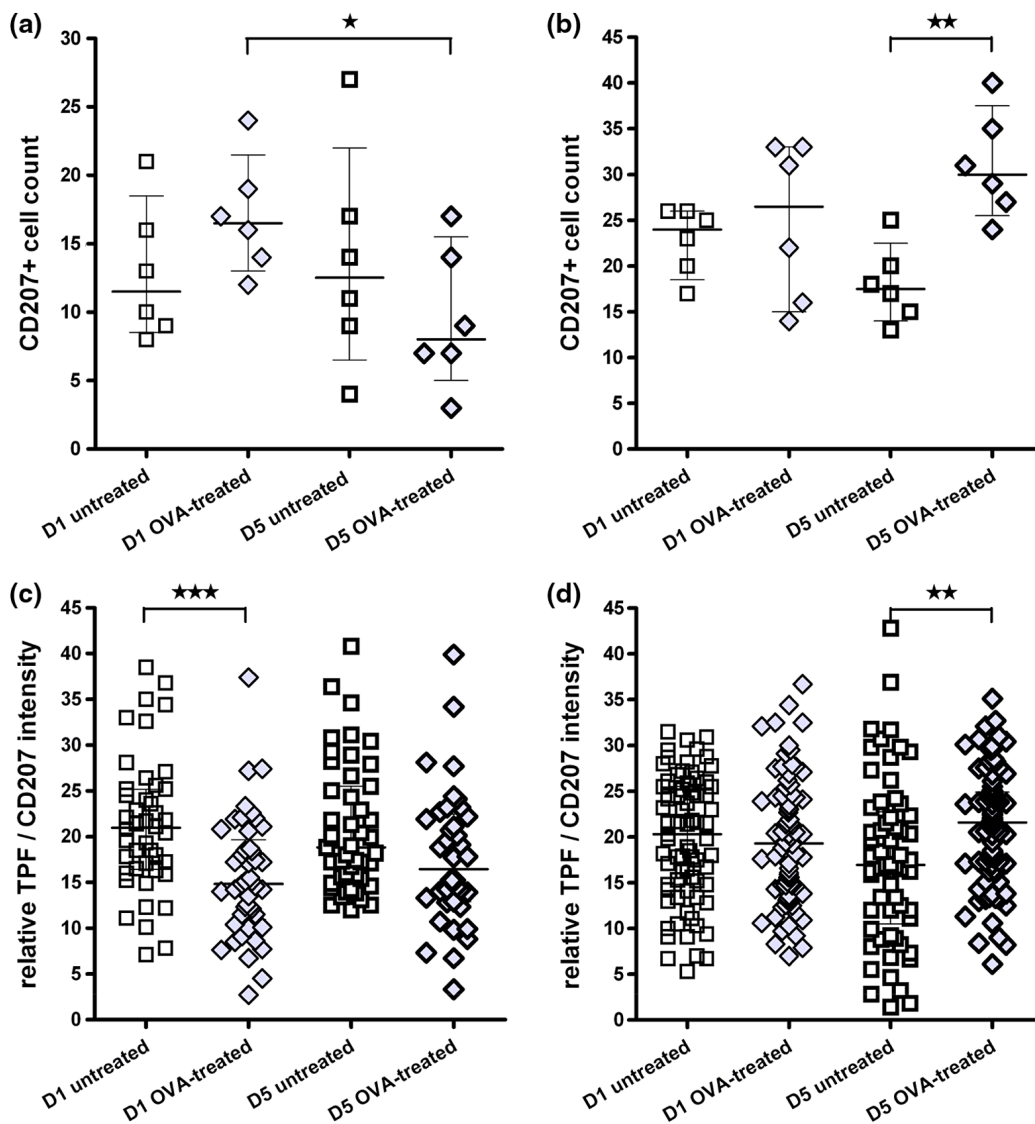


Fig. 5 Comparison of the number of CD207-positive LCs and the expression of CD207 between the D1, D5, and between the OVA-untreated and OVA-treated skin: (a) The number of CD207-positive LCs within skin. The number of D5 OVA-treated skin is decreased compared to that of D1; (b) the number of CD207-positive LCs within DLN. The number of D5 OVA-treated side is increased compared to that of the D5 untreated side; (c) the relative expression of CD207 on LCs within skin. On D1, the relative expressions of OVA-treated side skin are decreased compared to that of untreated side; (d) the relative expression of CD207 on LCs within DLN. Note that on D5, the relative expressions of OVA-treated DLN are increased than those of untreated side. Data are expressed as median (horizontal lines) and interquartile range (the range of values between the 25th and 75th percentile of distribution). Counting area: 120x120 μm . * $P < 0.05$, ** $P < 0.01$, *** $P < 0.001$. Data are representatives of three experiments.

from the DLN specimens from the mice that received EC sensitization on day one (D1) and on day five (D5), respectively. A total of 10 images and six fields randomly chosen within each image were selected from each mouse for analysis. Multiple measurements of the same image are counted as independent samples. In brief, optical sectioned images were saved as uncompressed 8-bit grayscale tiff files and analyzed using the NIH Image software program (NIH Image J 1.44). Signal levels were converted to a numerical value using a grayscale from 0 (white) to 255 (black). The background noise was subtracted from all acquired values. Cell numbers were measured using the Analyze→Analyze Particles function of ImageJ, where a single value is entered and particles smaller than that value are then ignored. We used 10 μm and particles (actually cells) smaller than that value were ignored.²⁰ To include every possible cell, we kept circularity at the default 0.00 to 1.00. Before analysis, we checked all the counted particles shown as numbered

outlines using the “show” function, and compared that with the original image. The density of LCs was also determined (cells/ mm^2). The quantitative analysis of TPF emitted from the Alexa Fluor 647-rat anti-mouse CD207 has been described previously.¹⁹ To account for variations in the grayscale intensity due to possible nonuniformity of skin and/or lymph node tissue, mean gray values (MGVs, average gray value within the region of interest) were measured to determine the levels of TPF.

2.5 Statistical Analysis

Data are expressed as mean \pm standard deviation, unless otherwise specified. The comparison of the cell counts and the relative TPF intensity among groups were expressed as median (the 50th percentile) and interquartile range (the range of values between the 25th and 75th percentile of distribution) and were statistically analyzed using a nonparametric Mann-Whitney

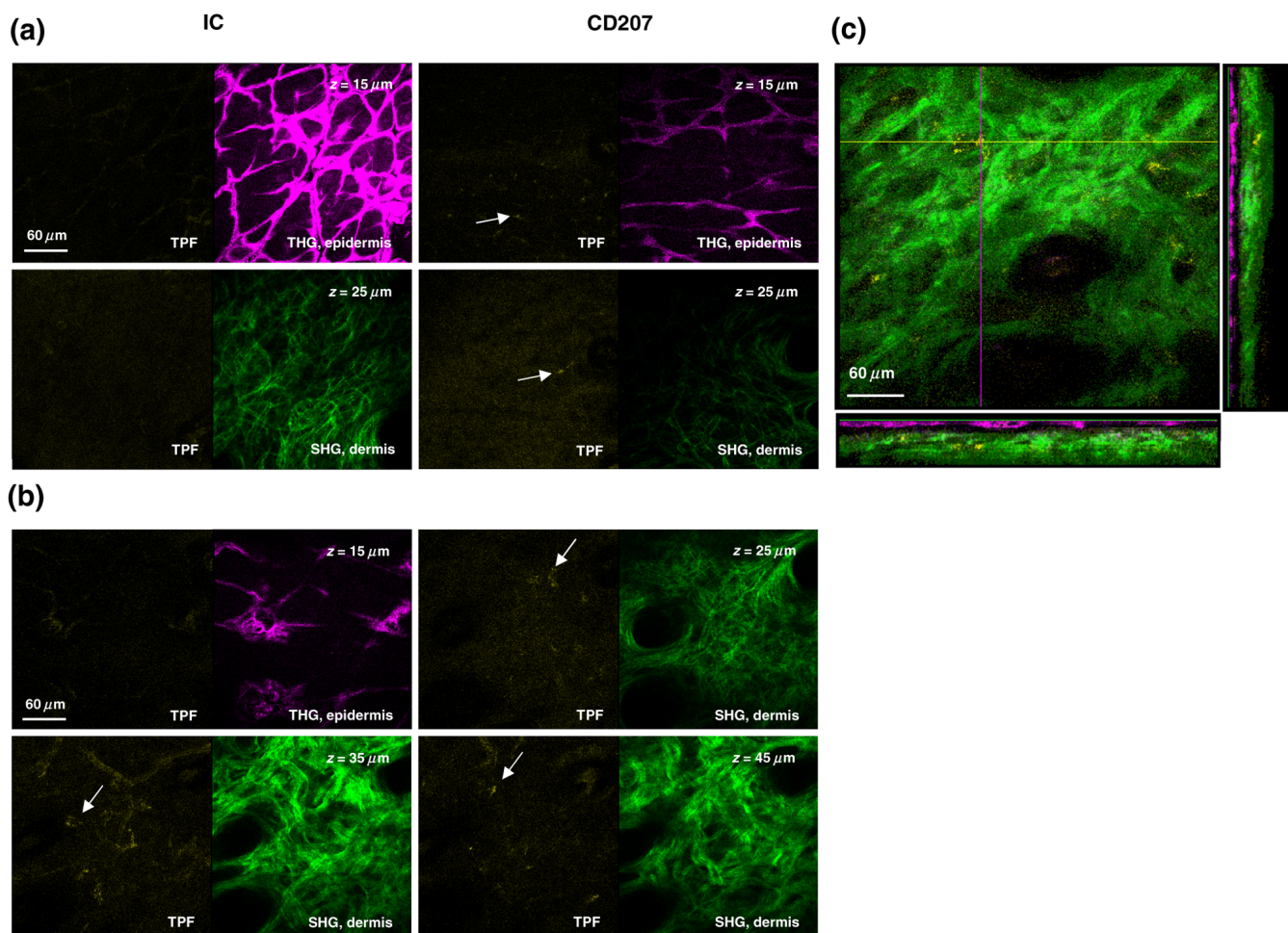


Fig. 6 Multimodal sectioning images from the surface of the skin of BALB/c mice received intraperitoneally injected Alexa Fluor 647-rat anti-mouse CD207 mAb *in vivo*. Images were acquired with the application of long-pass emitter LF635/LP-A-000; (a) The representative sequential images along the x - y plane of normal skin. The epidermis is mapped by THG (purple) signals. The dermis is mapped by SHG (green) signals. Simultaneous image of TPF signal, SHG signal, and THG signal are displayed. Some CD207⁺ cells are observed in the epidermis and few in the dermis (white arrow). In the isotype control (IC) group, no TPF signals of CD207⁺ cells are observed in both epidermis and dermis. z = depths in μm measured from skin surface; (b) the representative sequential images along the x - y plane of D1 OVA-treated skin. No CD207⁺ cells are observed in the epidermis. In contrast, some yellow signals representing TPF from CD207⁺ cells (white arrow) are detected within the dermis of the D1 OVA-treated skin; (c) the representative x - z plane sectioning images from the whole layer of D1 OVA-treated skin. The epidermis is mapped by THG (purple) signals. The dermis is mapped by SHG (green) signals. The sectioning images along x - y plane as indicated by purple and yellow lines are shown on the right and bottom side, respectively. The characteristic distribution of the yellow TPF signals representing CD207⁺ cells located within dermis was noted. Data are representative image of three mice. Scale bar: 60 μm .

U test. All statistical analyses were performed with Prism software (Graph Pad, San Diego, CA). A *P* value of less than 0.05 was considered to indicate a statistically significant difference.

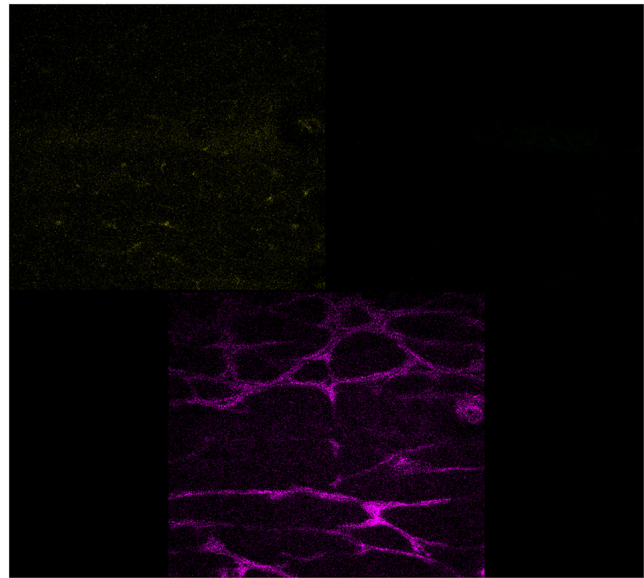
3 Results

3.1 Observation of MHC Class II Expressing Cells Labeled with Alexa Fluor 700-Rat Anti-mouse MHC Class II mAb

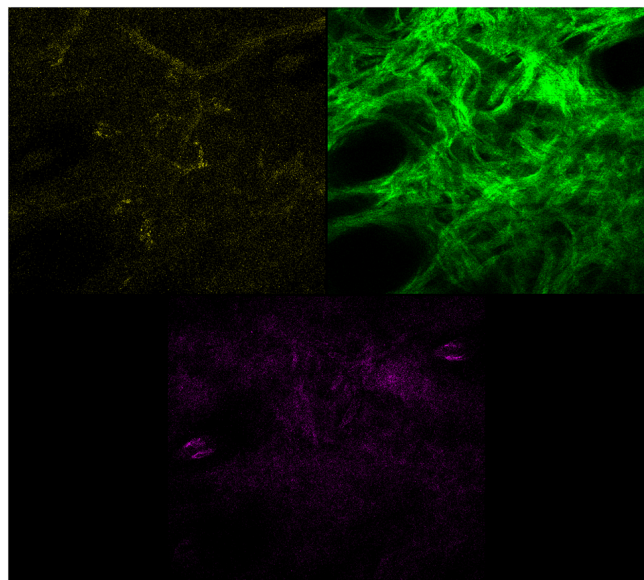
Human and mouse DCs in the epidermis are easily identified based on the surface expression of the MHC class II molecules. We took advantage of the nonlinear two-photon fluorescence (TPF) from Alexa Fluor 700 under an excitation wavelength of 1230 nm of the Cr:forsterite femto-second (fs) laser.^{19,21} A typical emission spectrum acquired from Alexa Fluor 700 conjugated mAb against MHC class II was measured [Fig. 1(a)]. We acquired sequential images along the *x-y* plane from the surface of the fixed skin. We found some red spot signaling located within the epidermis [Fig. 2(a) to 2(c)]. We confirmed the nonlinear signal by verifying that the TPF signals we observed had a central emission wavelength around 703 nm. We repeated our experiment *in vivo*. We observed the same characteristic distribution of red spot signals outlining some cellular morphology within the epidermis [Fig. 2(d) to 2(e)]. We measured the *xz*-sectioned nonlinear images in the skin of live mice and confirmed that these red spot signals were located at the basal epidermis [Fig. 2(f)]. Next we examined intact lymph nodes by Cr:forsterite laser-based nonlinear microscopy to determine their suitability for lymph nodes imaging. We acquired sequential images along the *z*-axis from the surface of the fixed DLN. Some red signals representing the TPF from the Alexa Fluor 700-rat anti-mouse MHC Class II molecules were present in the inner paracortex area, a T cell-rich zone (Fig. 3).^{22,23} Deduced from their locations, these brightly stained cells within skin and DLN might be some MHC class II expressing cells, including DCs and LCs.

3.2 Observation of CD207 Expressing LCs Labeled with Alexa Fluor 647-Rat Anti-mouse CD207 mAb

CD207 is a marker that persists during LC maturation and migration and can therefore be used as a tracer.²² By intraperitoneally injecting Alexa Fluor 647-rat anti-mouse CD207 mAb into mice as our fluorescent probe, we could trace the TPF signal from Alexa Fluor 647. A typical emission spectrum acquired from the skin surface is shown in [Fig. 1(b)]. We acquired sequential sectioned images along the *x-y* plane from the surface of the fixed skin and found some cells with extending dendrites located within the epidermis (Fig. 4 and Video 1). We confirmed the nonlinear signal by verifying that the TPF signals we observed had a central emission wavelength around 677 nm. To verify the specificity of the labeling of CD207 and of the imaging of LCs, we use the Alexa Fluor 647-rat IgG2a isotype control (IC) mAb. We did not observe any fluorescent signals representing the TPF from the fluorescent dye Alexa Fluor 647 in the mice group receiving IC mAb (data not shown). We found that the average size of the cell body of LCs was $13.44 \pm 3.15 \mu\text{m}$. The average epidermal LC density was $1116.7 \pm 127.8 \text{ cells/mm}^2$, similar to the reported value of $1052 \pm 109 \text{ cells/mm}^2$.^{20,22} We verified that our technique could specifically image and trace the LCs *in situ*, aiding to



Video 2 *In vivo* movies of depth-resolved *x-y* plane sectioning images from the normal skin of BALB/c mice received Alexa Fluor 647-rat anti-mouse CD207 mAb. The epidermis is mapped by THG (purple) signals. The dermis is mapped by SHG (green) signals. The CD207-expressing LCs was mapped by TPF (yellow) signals. Simultaneous image of TPF signal (upper left, yellow color), SHG signal (upper right, green color), and THG signal (lower central, purple color) are displayed. Most of CD207-expressing LCs are observed in the epidermis and a few in the dermis (MOV, 255 KB) [URL: <http://dx.doi.org/10.1117/1.JBO.17.11.116007.2>].



Video 3 *In vivo* movies of depth-resolved *x-y* plane sectioning images from the D1 lesional skin of BALB/c mice received Alexa Fluor 647-rat anti-mouse CD207 mAb. The epidermis is mapped by THG (purple) signals. The dermis is mapped by SHG (green) signals. The CD207-expressing LCs is mapped by TPF (yellow) signals. Simultaneous image of TPF signal (upper left, yellow color), SHG signal (upper right, green color), and THG signal (lower central, purple color) are displayed. No CD207-expressing LCs are observed in the epidermis while many CD207-expressing LCs are detected within the dermis (MOV, 749 KB) [URL: <http://dx.doi.org/10.1117/1.JBO.17.11.116007.3>].

investigate the maturation and migration process of LCs under the real physiological and pathological conditions.

3.3 Comparison of Cellular Counts and Relative CD207 Expression of LCs Between OVA-Treated and OVA-Untreated Skin and DLNs

LCs may have an important role in the initiation of AD.²⁴ We use OVA EC sensitization to induce an inflammatory skin mimic AD to explore the role of CD207-expressing LCs in the initiation of allergen induced skin sensitization. We used the *x-y*-plane nonlinear images taken from fixed skin and lymph node samples of mice received EC sensitization and Alexa Fluor 647-rat anti-mouse CD207 mAb for quantitative analysis. The LC counts and the relative expression levels of CD207 represent by relative TPF intensity measured by optical analysis of the acquired images were compared [Fig. 5(a) to 5(d)].

LC counts in skin and DLNs. We observed decreased counts of epidermal CD207⁺ LCs in D5 OVA-treated skin compared to D1 OVA-treated skin (D5 treated versus D1 treated $P < 0.05$) [Fig. 5(a)]. We observed an increased number of LCs in DLN of OVA-treated skin on D5 (D5 treated versus D5 untreated $P < 0.005$) [Fig. 5(b)]. Our result indicated that both the decreased CD207⁺ LCs within the OVA-treated skin and the increased CD207⁺ LCs arrived the DLNs were associated with the dynamic migration of CD207⁺ LCs after OVA-induced EC sensitization.

Relative CD207 expressions in skin and DLNs. The relative CD207 expression in the OVA-treated skin was decreased compared to that in the OVA-untreated skin on D1 (D1 treated versus D1 untreated $P < 0.001$) [Fig. 5(c)]. The relative CD207 expression levels in the DLNs of OVA-treated skin were increased on D5 (D5 treated versus D5 untreated $P < 0.05$) [Fig. 5(d)]. Our result indicated that both the decreased CD207 expression of LCs within the OVA-treated skin and the increased CD207 expression of LCs arrived the DLNs were relevant to the

functional phenotype of CD207⁺ LCs after OVA-induced EC sensitization.

3.4 In Vivo Imaging of CD207⁺ Cells Within Normal and D1 OVA-Treated Skin

To determine whether we could trace and image the CD207⁺ LCs *in vivo*, we intraperitoneally injected Alexa Fluor 647-rat anti-mouse CD207 mAb into mice, and sectioned images were acquired 6 h later. We observed some LCs within the epidermis of OVA-untreated mice [Fig. 6(a) and Video 2], but we did not find any LCs in the epidermis of mice received injection of Alexa Fluor 647-rat IgG2a IC mAb [Fig. 6(a)].

In the following experiment we selected the long-pass emitter LF635/LP-A-000 to specifically collect the fluorescent signals of emission wavelength > 650 nm, e.g., those from Alexa Fluor 647-rat anti-mouse CD207 mAb (peak emission wavelength = 677 nm under excitation wavelength 1230 nm), and to omit the signals from SHG with emission wavelength = 615 nm.¹⁹ Thus we were able to more specifically collect the fluorescent signals emitted from the Alexa Fluor 647-rat anti-mouse CD207 mAb; thus we were suitable for explore the physiological conditions within the dermis which were mapped by SHG. When we observed the epidermis of D1 OVA-treated skin, we found nearly no CD207⁺ LCs in the epidermis; however, there were CD207⁺ cells intercalated among collagen fibers [Fig. 6(b) and Video 3]. We acquired the *x-y* and *x-z* plane sectional images simultaneously and found that the CD207-expressing cells were located within the superficial layer of the dermis [Fig. 6(c) and Video 3]. Interestingly, Soumelis et al. reported that many CD207⁺ LCs were found only within the epidermis of normal skin while many CD207-expressing DCs were found within the dermis of lesional skin.²⁵ Similar patterns of distribution of CD207⁺ cells were observed in our experiment, suggesting that these cells may be epidermal CD207⁺ LCs that migrated to the dermis

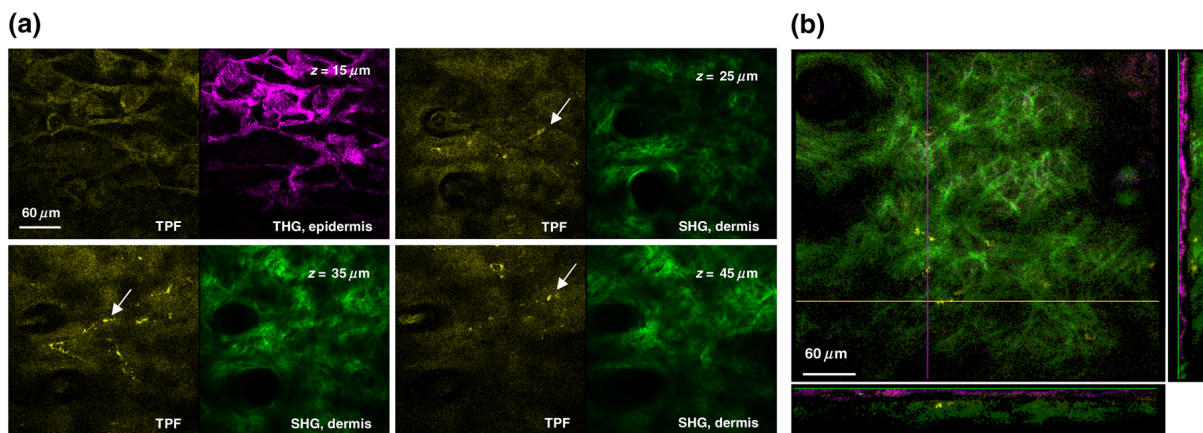
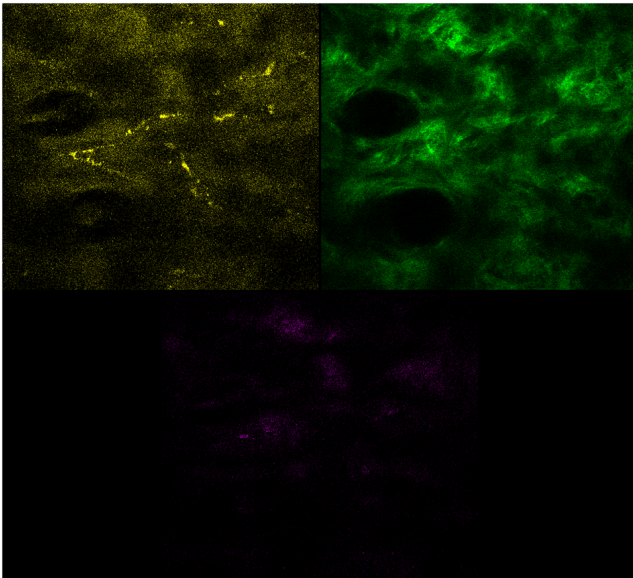


Fig. 7 Multimodal sectioning images from the surface of the skin of BALB/c mice received intraperitoneally injected OVA-Alexa Fluor 647 conjugate *in vivo*. Images were acquired with the application of the long-pass emitter LF635/LP-A-000; (a) the representative sequential images along the *x-y* plane. The epidermis is mapped by THG (purple) signals. The dermis is mapped by SHG (green) signals. Simultaneous image of TPF signal, SHG signal, and THG signal are displayed. No OVA-carrying cells are observed in the epidermis due to lack of TPF signal from OVA-Alexa Fluor 647 conjugate. In contrast, some yellow TPF signals representing OVA-carrying cells are detected within the dermis of skin (white arrow). SHG (second harmonic generation); THG (third harmonic generation); TPF (two-photon fluorescence); (b) the representative *x-z* plane sectioning images from the whole layer of skin. The epidermis is mapped by THG (purple) signals. The dermis is mapped by SHG (green) signals. The sectioning images along *x-y* plane as indicated by the purple and yellow lines are shown on the right and bottom side, respectively. The characteristic distribution of the yellow TPF signals representing OVA-capturing cells located within dermis is noted. Data are representative image of three mice. Scale bar: 60 μm . z = depths in μm measured from skin surface.



Video 4 *In vivo* movies of depth-resolved x - y plane sectioning images from the abdominal skin of BALB/c mice received OVA-Alexa Fluor 647. The epidermis is mapped by THG (purple) signals. The dermis is mapped by SHG (green) signals. The OVA-carrying cells are mapped by TPF (yellow) signals. Simultaneous image of TPF signal (upper left, yellow color), SHG signal (upper right, green color), and THG signal (lower central, purple color) are displayed. No OVA-carrying cells are observed in the epidermis. In contrast, some OVA-carrying cells are detected within the dermis of skin (MOV, 963 KB) [URL: <http://dx.doi.org/10.1117/1.JBO.17.11.116007.4>].

or the occurrence of dermal CD207⁺ DCs within the OVA sensitized skin.

3.5 *In Vivo* Imaging of OVA Within Normal Skin and *Ex Vivo* Imaging of OVA in Skin DLNs

In an attempt to directly measure the antigen capturing capabilities of DCs *in vivo*, we administered OVA-Alexa Fluor 647 conjugate into BALB/c mice via the intraperitoneal route, and sectioned images were acquired 6 h later. Again, we use the long-pass emitter LF635/LP-A-000 to specifically collect the fluorescent signals emitted from the OVA-Alexa Fluor 647 conjugate under the physiological conditions. We did not observe any fluorescent signal from the epidermis; however, we did find many clusters of fluorescent signals from the OVA-Alexa Fluor 647 conjugate within the dermis [Fig. 7(a) and Video 4]. We acquired the x - y and x - z plane sectional images simultaneously and found that these OVA were located within the superficial dermis [Fig. 7(b)]. Recently, it has been reported that after subcutaneous injection of FITC-OVA probes, which accumulated in dermal cells but not in epidermal cells.²⁶ Our approach showed the similar result that redistribution of systemic sensitizing Ag into skin were within the dermis.

We then observe the excised skin DLNs *ex vivo* and found many signals of OVA-Alexa Fluor 647 conjugate from the cells within outer and inner paracortex (Fig. 8 and Video 5), suggesting the accumulated OVA-carrying cells within the DLNs after application of OVA-Alexa Fluor 647 conjugate.²³ Thus we confirmed that Cr:forsterite laser-based nonlinear microscopy

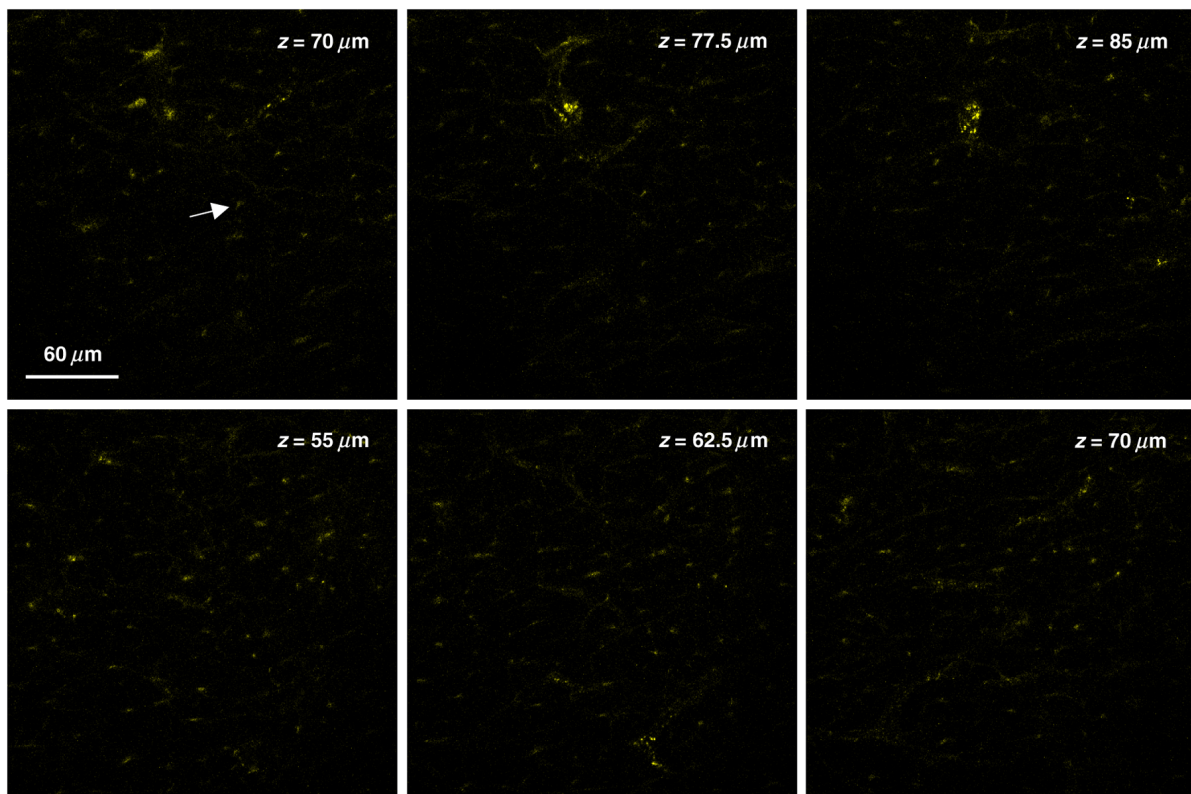
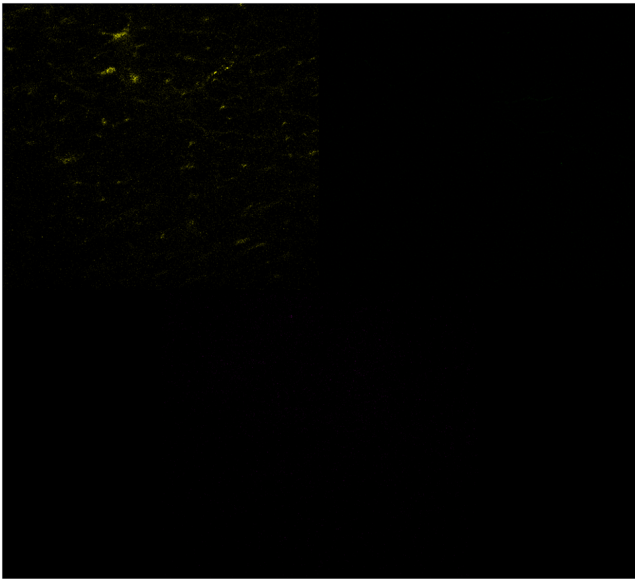


Fig. 8 Multimodal sequential sectioning images along the x - y plane at various depths of the fixed skin-draining lymph node of BALB/c mice received intraperitoneally injected Ovalbumin-Alexa Fluor 647 conjugate *in vivo*. Images were acquired with the application of the long-pass emitter LF635/LP-A-000. Images of the upper and lower row are from different skin-draining lymph node. Note the yellow TPF signals representing CD207-expressing LCs are detected within the skin-draining lymph node (white arrow). z = depths in μm measured from the surface of capsule. Data are representative image of three mice. Scale bar: 60 μm .



Video 5 *Ex vivo* movies of depth-resolved x-y plane sectioning images from the skin DLN of BALB/c mice received OVA-Alexa Fluor 647 conjugates. Simultaneous image of TPF signal (upper left, yellow color), SHG signal (upper right, green color), and THG signal (lower central, purple color) are displayed. The capsule is mapped by some THG signal representing the epithelium and few SHG signals representing the connective tissue. The honeycomb shape area within the capsule might be the adipose tissue surrounding the connective tissue of capsule. Following the capsule, there is an area showing dense and light TPF signal of OVA-Alexa Fluor 647 conjugates from the dermal DCs within the outer paracortex.²³ Following the outer paracortex, there is an area showing sparse and dim TPF signal of OVA-Alexa Fluor 647 conjugates from the migratory LCs within the inner paracortex²³ (MOV, 521 KB) [URL: <http://dx.doi.org/10.1117/1.JBO.17.11.116007.5>].

complemented with exogenous fluorescent probe could detect the antigen-carrying cells or the occurrence of antigen within skin and LNs.

3.6 Co-Localization of OVA with CD205-Expressing Dendritic Cells in Skin DLNs

CD207 was frequently co-expressed with CD205.²⁷ We first injected Alexa Fluor 700-rat anti-mouse CD205 mAb intraperitoneally and injected OVA-Alexa Fluor 647 conjugate 6 h later. We used the long-pass emitter E700lp to collect the fluorescent signals emitted from the Alexa Fluor 700-rat anti-mouse CD205 mAb (peak emission wavelength = 703 nm under excitation wavelength 1230 nm), and the short-pass emitter E700sp-2p to collect the fluorescent signals emitted from the OVA-Alexa Fluor 647 conjugate. We found that the yellow signal from OVA-Alexa Fluor 647 conjugate were adjacent to the red signal from Alexa Fluor 700-rat anti-mouse CD205 mAb (Fig. 9 upper panel). When we merged the images obtained from different emitters, we observed that there was an overlap between populations of cells expressing CD205 and populations of OVA-capturing cells in most of field (Fig. 9, lower panel), implying that CD205⁺ cells co-expressing CD207 are capable of uptake OVA-Alexa Fluor 647 conjugate and transport it to the DLN for initiation of the specific T cell immune response.

4 Discussion

There are two major methods for *in vivo* imaging of live tissues, cells, or molecules. One approach is to introduce fluorescent proteins YFP or GFP, which selectively target the tissue of interest in transgenic mice to highlight various cellular or molecular features.²⁸ The other approach is to take advantage

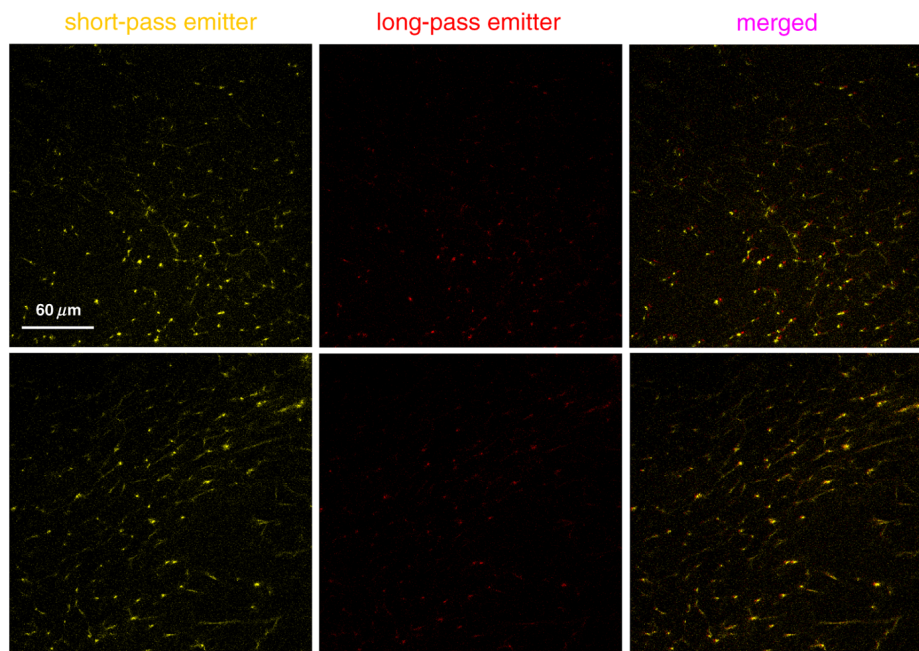


Fig. 9 Co-localization of OVA-Alexa Fluor 647 conjugate with Alexa Fluor 700-rat anti-mouse CD205 labeled DCs within the skin-draining lymph nodes. The TPF signal (yellow color) emitted from OVA-Alexa Fluor 647 conjugate with a wavelength below 700 nm are collected by the short-pass emitter E700sp-2p. The TPF signal (red color) emitted from Alexa Fluor 700-rat anti-mouse CD205 labeled DCs with a wavelength above 700 nm are collected by the long-pass emitter E700lp. The upper panel shows an artificial “shift” when image were acquired from two different emitters. Note the yellow and red fluorescent signals are nearly total merged in the lower panel images. Images of the upper and lower panel are from different skin-draining lymph node. Data are representatives of three experiments.

of endogenous molecules (e.g., NADPH), which provides valuable information on the tissue architecture without the need for exogenous labeling.²⁹ The drawback of the fluorescent proteins method is the inability to quantify the expression levels of molecules of interest. The endogenous molecules method lacks specificity, and only limited molecules are available. Our technique provides two levels of specificity. First, the molecules are specifically recognized by the mAb, and the nonspecific binding effects of the Alexa Fluor 647-rat anti-mouse CD207 were controlled because no LCs were seen within the Alexa Fluor 647-rat IgG2a isotype control mAb group [Fig. 6(a)]. Second, only the limited exogenous fluorophores (e.g., Alexa Fluor 647) are excited under Cr:forsterite laser-based nonlinear microscopy because much of the autofluorescence from endogenous fluorophores was reduced.¹⁹ Our method is a promising approach that could be used to unequivocally identify and track CD207⁺ LCs by *in vivo* imaging. We were limited by the fact that the resolution of some images shown appears rather low. Besides, we could stain CD207⁺ LCs in fixed skin samples (Fig. 4), but only a few CD207⁺ LCs in skin of live mice (Fig. 6). The reason was fluorescence changes associated with tissue fixation.¹⁹ This discrepancy of imaging reflects the difference in biophysical properties of epidermis between the live and the dead/fixed skin of mice, hence the different TPF intensities from CD207 mAb-conjugated Alexa Fluor 647.

Prerequisite roles of skin DCs and potentially of LCs in the development of AD have been suggested.²⁴ An increase in LC proliferation has been reported to be required to induce the Th2 polarization of CD4⁺ T cells and maintain disease.³⁰ Our data demonstrated an increased number of LCs in the DLNs in the later sensitization phase on D5.²³ The dynamic changes of LCs seen in our results are associated with the EC sensitization course. It is interesting to note that found some occurrences of migratory CD207⁺ LCs or dermal CD207⁺ DCs within the dermis of the mice. All published descriptions of dermal CD207⁺ DCs have so far been in the mouse.³¹ In the LC paradigm, no distinctions could be drawn between epidermal LCs *en route* through the dermis and the novel dermal CD207⁺ DCs *in situ*. It turned out that these dermal CD207⁺ DC in the dermis were a dermis-resident population, unrelated to LC, and they can be readily detected in the draining lymphoid organs called lymph-node-resident CD207⁺ DCs.³¹ Our results confirm a similar result in that a decrease and/or disappearance of LCs in the epidermis was directly correlated with the increased number of CD207⁺ LCs or dermal CD207⁺ DCs in the superficial dermis and in the DLNs.³² We suggest CD207⁺ LCs play some role in the initiation of OVA induced skin sensitization use EC sensitization.

Our model used here is only a model of epicutaneous sensitization induced inflammatory skin. Our study were similar to Spergel et al. that the epidermal layer was approximately three to five cell layers thick in OVA sensitized sites compared with two to three cell layers thick in saline sensitized sites.^{19,33} Although our model is different from the originally described model,³³ the epidermal hyperkeratosis/thickening and dermal fibrosis shown here indicated that our murine model shared the characteristic cutaneous inflammatory response associated with AD.

In our paper, we used Alexa Fluor fluorophores for molecular labeling and *in vivo* imaging, so the toxicity of Alexa fluor used should be addressed. A review of published literature on the toxicity of some widely used fluorophores was conducted by

searching 26 comprehensive biomedical and chemical literature databases and analyzing the retrieved material.³⁴ The Alexa Fluor fluorophores were searched without accompanying toxicity-related reports. Besides, no toxicity or developmental abnormalities resulting from treatment with Alexa Fluor 647 conjugate were observed in an *in vivo* imaging experiment of developing zebrafish.³⁵ The Alexa fluorophores we used were administrated into mice *in vivo*. However, applying these fluorophores and determining the safe dose of these fluorophores will require further clinical and laboratory investigation.

With Alexa-Fluor 647 conjugates used as a tracer, we showed the dynamic migration and functional phenotype of CD207⁺ cells and the existence and encounter of OVA. We showed that LCs are present in the skin and that they migrate to the DLN upon OVA induced EC sensitization. The distribution of OVA upon intraperitoneal injection and co-localization of OVA with CD207⁺ LCs in DLN has been readily demonstrated by our data. The respective data generated by Cr:forsterite laser-based multimodality nonlinear microscopy validate our method and the sensitization model, but also give new insights into that CD207 plays any role of allergen uptake in the development of allergic sensitization in human beings such as AD. Our approach using Cr:forsterite laser-based nonlinear microscopy complemented with an exogenous fluorescent probe demonstrates the potential to do flow cytometry and to perform immunohistochemistry (IHC) *in vivo*, which might be applied to real-time and specific detection of antigens/allergens and to evaluate the interaction between immune cells in the skin and in the lymph node *in vivo*.

Acknowledgments

The authors would like to acknowledge the support from the National Science Council of Taiwan under NSC 99-2314-B-002-024-MY3, the National Taiwan University Hospital under NTUH 099-001394 and the NTU Research Center for Medical Excellence.

References

1. D. Y. M. Leung and T. Bieber, "Atopic dermatitis," *Lancet* **361**(9352), 151–160 (2003).
2. E. B. Mitchell et al., "Increase in skin mast cells following chronic house dust mite exposure," *Br. J. Dermatol.* **114**(1), 65–73 (1986).
3. N. Novak, T. Bieber, and D. Y. M. Leung, "Immune mechanisms leading to atopic dermatitis," *J. Allergy Clin. Immunol.* **112**(6 Suppl.), S128–S139 (2003).
4. M. Merad, F. Ginhoux, and M. Collin, "Origin, homeostasis and function of Langerhans cells and other langerin-expressing dendritic cells," *Nat. Rev. Immunol.* **8**(12), 935–947 (2008).
5. K. Kerschenlohr et al., "Atopy patch test reactions show a rapid influx of inflammatory dendritic epidermal cells in patients with extrinsic atopic dermatitis and patients with intrinsic atopic dermatitis," *J. Allergy Clin. Immunol.* **111**(4), 869–874 (2003).
6. N. S. Stambach and M. E. Taylor, "Characterization of carbohydrate recognition by langerin, a C-type lectin of Langerhans cells," *Glycobiology* **13**(5), 401–410 (2003).
7. J. Valladeau et al., "The monoclonal antibody DCGM4 recognizes Langerin, a protein specific of Langerhans cells, and is rapidly internalized from the cell surface," *Eur. J. Immunol.* **29**(9), 2695–2704 (1999).
8. J. Valladeau et al., "Langerin, a novel C-type lectin specific to Langerhans cells, is an endocytic receptor that induces the formation of Birbeck granules," *Immunity* **12**(1), 71–81 (2000).
9. J. Valladeau et al., "Identification of mouse langerin/CD207 in Langerhans cells and some dendritic cells of lymphoid tissues," *J. Immunol.* **168**(2), 782–792 (2002).

10. K. Takahara et al., "Identification and expression of mouse Langerin (CD207) in dendritic cells," *Int. Immunol.* **14**(5), 433–444 (2002).
11. A. Ingber, "Langerhans cell receptors," *Dermatol. Clin.* **25**(4), 559–562 (2007), ix.
12. A. Elentner et al., "Langerhans cells are critical in the development of atopic dermatitis-like inflammation and symptoms in mice," *J. Cell. Mol. Med.* **13**(8B), 2658–2672 (2009).
13. L. Chorro et al., "Langerhans cell (LC) proliferation mediates neonatal development, homeostasis, and inflammation-associated expansion of the epidermal LC network," *J. Exp. Med.* **206**(13), 3089–3100 (2009).
14. N. Novak, W. Peng, and C. Yu, "Network of myeloid and plasmacytoid dendritic cells in atopic dermatitis," *Adv. Exp. Med. Biol.* **601**, 97–104 (2007).
15. T. Bieber, "Atopic dermatitis," *Ann. Dermatol.* **22**(2), 125–137 (2010).
16. L. Wang et al., "Langerin expressing cells promote skin immune responses under defined conditions," *J. Immunol.* **180**(7), 4722–4727 (2008).
17. T. Bieber, "Atopic dermatitis," *N Engl J Med.* **358**(14), 1483–1494 (2008).
18. A. H. Liu, "Innate microbial sensors and their relevance to allergy," *J. Allergy Clin. Immunol.* **122**(5), 846–858 (2008).
19. J. H. Lee et al., "Noninvasive *in vitro* and *in vivo* assessment of epidermal hyperkeratosis and dermal fibrosis in atopic dermatitis," *J. Biomed. Opt.* **14**(1), 014008 (2009).
20. W. J. Mulholland et al., "Multiphoton high-resolution 3D imaging of Langerhans cells and keratinocytes in the mouse skin model adopted for epidermal powdered immunization," *J. Invest. Dermatol.* **126**(7), 1541–1548 (2006).
21. C. K. Sun, "Higher harmonic generation microscopy," *Adv. Biochem. Eng. Biotechnol.* **95**, 17–56 (2005).
22. P. Stoitzner et al., "Visualization and characterization of migratory Langerhans cells in murine skin and lymph nodes by antibodies against Langerin/CD207," *J. Invest. Dermatol.* **120**(2), 266–274 (2003).
23. A. Kissenpennig et al., "Dynamics and function of Langerhans cells *in vivo*: dermal dendritic cells colonize lymph node areas distinct from slower migrating Langerhans cells," *Immunity* **22**(5), 643–654 (2005).
24. S. Dubrac, M. Schmuth, and S. Ebner, "Atopic dermatitis: the role of Langerhans cells in disease pathogenesis," *Immunol. Cell Biol.* **88**(4), 400–409 (2010).
25. V. Soumelis et al., "Human epithelial cells trigger dendritic cell mediated allergic inflammation by producing TSLP," *Nat. Immunol.* **3**(7), 673–680 (2002).
26. R. E. Frugé et al., "Real-time visualization of macromolecule uptake by epidermal Langerhans cells in living animals," *J. Invest. Dermatol.* **132**(3 Pt 1), 609–614 (2012).
27. S. Henri et al., "The dendritic cell populations of mouse lymph nodes," *J. Immunol.* **167**(2), 741–748 (2001).
28. R. Weigert et al., "Intravital microscopy: a novel tool to study cell biology in living animals," *Histochem. Cell Biol.* **133**(5), 481–491 (2010).
29. W. R. Zipfel et al., "Live tissue intrinsic emission microscopy using multiphoton-excited native fluorescence and second harmonic generation," *Proc. Natl. Acad. Sci. U.S.A.* **100**(12), 7075–7080 (2003).
30. L. Chorro et al., "Langerhans cell (LC) proliferation mediates neonatal development, homeostasis, and inflammation-associated expansion of the epidermal LC network," *J. Exp. Med.* **206**(13), 3089–3100 (2009).
31. N. Romani, B. E. Clausen, and P. Stoitzner, "Langerhans cells and more: langerin-expressing dendritic cell subsets in the skin," *Immunol. Rev.* **234**(1), 120–141 (2010).
32. S. Taweechaisupapong et al., "Langerhans cell density and serological changes following intradermal immunisation of mice with dengue 2 virus," *J. Med. Microbiol.* **45**(2), 138–145 (1996).
33. J. M. Spergel et al., "Epicutaneous sensitization with protein antigen induces localized allergic dermatitis and hyperresponsiveness to methacholine after single exposure to aerosolized antigen in mice," *J. Clin. Invest.* **101**(8), 1614–1622 (1998).
34. R. Alford et al., "Toxicity of organic fluorophores used in molecular imaging: literature review," *Mol. Imaging.* **8**(6), 341–354 (2009).
35. S. T. Laughlin et al., "*In vivo* imaging of membrane-associated glycans in developing zebrafish," *Science* **320**(5876), 664–667 (2008).